COMBUSTION INSTABILITIES ANALYSIS BASED ON THE FLAME DESCRIBING FUNCTION APPLIED TO SWIRLING FLAMES

Paul Palies*[1], Daniel Durox[1], Thierry Schuller[1] and Sebastien Candel[1]

[1] EM2C Laboratory at CNRS and Ecole Centrale Paris
Grande Voie des Vignes, 92 295 Chatenay-Malabry, France
* Corresponding author: paul.palies@em2c.ecp.fr

Thermoacoustic instabilities are analyzed by making use of a nonlinear representation of flame dynamics based on the describing function. In this framework, the flame response is determined as a function of frequency and amplitude of perturbations impinging on the combustion region. This methodology is applied to confined swirling flames in a laboratory scale setup (2.5 to 4 kW) comprising an upstream manifold, an injection unit equipped with a swirler (swirl number = 0.55) and a cylindrical flame tube. The flame describing function is experimentally determined and is combined with an acoustic transfer matrix representation of the system to provide growth rates and oscillation frequencies as a function of perturbation amplitude. These data can be used to determine regions of instability, frequency shifts with respect to the acoustic eigenfrequencies and they also yield amplitude levels when self-sustained oscillations of the system have reached a limit cycle. This equilibrium is obtained when the amplitude dependent growth rate equals the damping rate in the system. This requires an independent determination of this last quantity which is here based on measurements of the resonance response curve. Results obtained are compared with observations from systematic experiments carried out by varying the test combustor geometry. The demonstration of the FDF framework in a generic configuration indicates that this can be used in more general situations of technological interest.

Introduction

Research on combustion instabilities has been quite intense during the recent period in relation with the development of lean premixed combustors but prediction of these phenomena at the design stage still constitutes a challenge. It is known that high performance combustors feature instabilities which are mainly driven by the unsteady heat release rate. In these modes, heat release rate fluctuations are generally delayed with respect to incident perturbations and give rise to an unstable growth of oscillations [1–3]. These perturbations can be generated in many different ways, but in most cases they are associated with convection of hydrodynamic perturbations [4] or fluctuations of the mixture composition [5].

The standard analysis of combustion instability combines the transfer function of the flame with a description of the system acoustics to determine eigenmodes and growth rates. Previous investigations indicate that it is possible to find the linear stability map of various types of burners but this is restricted to small perturbations and cannot account for the limit cycle oscillations observed in practice. It is well known that nonlinear mechanisms dominate the dynamics of real systems. These nonlinearities determine the limit cycle amplitudes, instability triggering (the mechanism by which an unstable oscillation

appears when the system experiences a finite amplitude perturbation), mode switching (the change in frequency observed during operation of practical devices) and hysteresis [6–9]. It has been shown recently that these combustion dynamics nonlinearities could be represented with a unified framework [10] in which the flame transfer function (FTF) is replaced by a flame describing function concept (FDF) which depends on the amplitude of perturbations impinging on the flame. A frequency domain stability analysis then yields growth rates and frequencies which depend on amplitude. Application of the FDF to the analysis of the stability of an unconfined [10] or confined [11] multipoint injection laminar burner indicates that it is possible to predict with reasonable accuracy many of the phenomena listed previously.

The FDF framework is here extended to deal with the dynamics of turbulent flames formed by a swirling injector in a confined geometry. Swirling injection is used in many practical systems like jet engines or gas turbine combustors. The swirling flow stabilizes combustion in a compact central reactive region. Swirling injection is usually adopted to anchor lean premixed combustion but the corresponding flow is highly unsteady and sensitive to acoustic perturbations eventually leading to combustion instabilities. The analysis of these instabilities has mainly been carried out with linear models [12, 13]. One of the issues in a nonlinear treatment is to suitably describe the swirling flame dynamics when flow perturbations have a variable level. The difficulty is compounded because the flame structure is complex with a central recirculation zone [14, 15] and flame folding phenomena take place at large amplitude levels [16]. It is known from some previous studies that much can be learnt by examining the flame response to incident velocity perturbations. Studies carried out on laminar “V" flame geometries [17] are useful to understand the dynamics of more complex flames, because they illustrate some fundamental interactions like that taking place between the flame sheet and vortices shed from the injector lip. These studies indicate that a “V" flame acts as an amplifier in the low frequency range. Incomplete flame transfer functions are available for turbulent “V" flame configurations [18] and for an unconfined “V" flame [20] showing the interactions between the flame front and the vortices. The case of swirling flames is less well documented. Some results are presented in [19]. A more complete study is presented in [16] but the swirl number is only estimated ($S = 1$). It is shown in this study that the unsteady shape of the flame is a strong function of the mass flow rate oscillation level. It is not easy to determine a time delay between flow rate fluctuations and resulting heat release rate perturbations. In a low swirl combustor study, there are some indications [21] that the dynamics of the flame is only weakly influenced by the swirl number but it is also found [16] that combustion dynamics of swirling flames feature an oscillation in the position and strength of the vortex breakdown. It is also indicated in [22] that the combustor inlet temperature affects the flame structure leading to different shapes and flame dynamics. Some data indicate that the response saturates when the mass flow rate fluctuation is augmented. Experimental and numerical transfer function of swirling flames are reported in [23, 24] for a frequency range extending from 0 to 400 Hz but effects of velocity perturbation amplitude are not documented and nonlinear effects are not characterized. It is however interesting to note that the transfer function features maximum and minimum gain values in the low frequency range. A theoretical model based on the vorticity transport equation [24] yields transfer functions which match those obtained with two different swirlers of radial and axial types. With the exception of references [16, 25, 26] there are few papers dealing with the nonlinear effect of flow modulations on the dynamics of confined swirling flames. It is found that as the amplitude of the instability grows, nonlinear saturation limits the level of heat release rate fluctuations and changes the phase of these fluctuations with respect to the incoming perturbations [16].

Well controlled experiments are reported in recent articles [27–29] where the dynamics of confined swirling flames is characterized by measurements of the FDF and by an examination of flame patterns during the cycle of oscillation at various levels of external modulation. These data will be used in what follows to develop a nonlinear analysis of combustion instabilities based on the FDF framework which combines a standard acoustic transfer matrix analysis of the different components forming the system with a nonlinear description of the flame response.

Predictions are obtained for an idealized system including an upstream manifold, an injection unit equipped with a swirler and a cylindrical tube confining the flame. In a different set of experiments,

the damping level is deduced from measurements of the resonant response to external modulations. The limit cycle amplitudes are then determined by searching the levels of perturbation for which the growth rate equals the damping rate. Numerical predictions are compared with experimental results corresponding to different geometrical parameters of the test configuration obtained by varying the lengths of the manifold and flame tube.

At this point, it is interesting to briefly review the possible approaches of combustion instability analysis and link the present framework to the other current tools. It is possible to distinguish three general classes : (a) Methods based on an acoustic analysis of the system relying on networks of elements and employing a linear transfer function to describe the flame response [30–32], (b) Methods based on a projection on the eigenmodes of the system leading to a set of differential equations for the modal amplitudes [33], (c) Direct methods where Large Eddy Simulations of the complete 3D, compressible Navier-Stokes equations are integrated [34] and the stability of the system is determined by observing the growth or decay of perturbations. The present approach extends the linear techniques of the first group by making use of the describing function concept [10]. As in standard linear analysis, the frequency and growth rate are obtained from a dispersion relation and the calculation is carried out in the frequency domain but the dispersion relation here depends on the amplitude of perturbations impinging on the flame. It is thus possible to see how the level affects the growth rate, determine the stability of the system by comparing this rate with the damping coefficient and find the level of oscillation at the limit cycle when the system is unstable.

This article begins with a description of the experimental configuration (section 2). Experimental data obtained for the describing function of swirling flames are reviewed in section 3. The theoretical model is outlined in section 4. Experimental determination of the system acoustic damping is described in section 5 together with predictions of self-sustained combustion oscillations of the system. This section also contains a comparison between experiments and calculations.

1 Experimental configuration

The combustor comprises an upstream manifold including a settling chamber, a contraction ended by a constant diameter duct equipped with the swirler, a horizontal end piece and a cylindrical flame tube (Fig. 1). A driver unit (loudspeaker) may be placed at the back end of this system to measure the flame describing function. An air/methane premixed flow is delivered to the premixing unit through two diametrally opposed apertures. The flow then crosses a grid and a honeycomb to break the largest turbulent scales. The gas then traverses a convergent unit to decrease the boundary layer thickness, reduce the level of turbulence and generate a flat velocity profile at the swirler inlet. The flow rotation is generated by the swirler which comprises eight twisted vanes arranged periodically around a central rod (6 mm in diameter). This central rod is terminated with a small cone (10 mm in diameter at its base) which stabilizes the flame during the unsteady motion of the flow. In this way, flashback is minimized. To keep the turbulence intensity low, the swirler blades use NACA four digits wing sections. The objective was to ensure that the level of fluctuations be less than the level of disturbance imposed by acoustic modulations. The result of the design process is a swirler comprising eight vanes periodically spaced with a stagger angle of 45°. The vane section is that of a NACA 8411 airfoil. The swirler has twisted vanes, so that the angle at the trailing edge evolves linearly from 30° at the hub to a value of 58° at the vane tip. Twisting is employed in order to impose the same rotation to the flow at all locations along the vane. The swirler was fabricated by fast prototyping of plastic material.The outer diameter of the injector is 22 mm. The swirler geometry was designed to obtain a predetermined value of the swirl number corresponding to a flow featuring an inner recirculation zone. Experimental profiles of axial and azimuthal velocities provide an estimate of the swirl number of about 0.55, see [29]. The tube confining the flame is made of quartz allowing optical access and transmitting the flame radiation in the near ultraviolet. Its diameter is 70 mm and the length l_3 can take different values : 100 mm, 150 mm, 200 mm and 400 mm respectively. There are also three lengths l_1 available for the upstream manifold : short (117.3 mm), medium (181.3 mm) and long (245.3 mm). The upstream manifold diameter is 65 mm. The length of

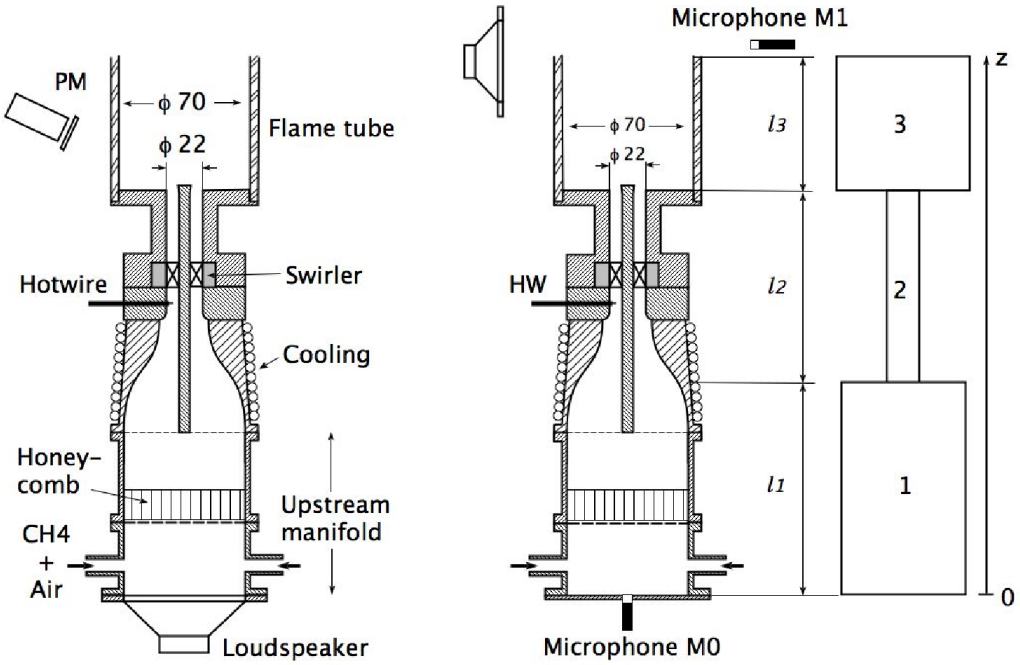

(a) (b) (c)

Figure 1: (a) : Experimental configuration used to measure flame describing functions. (b) : Without the loudspeaker, this setup is also used to obtain frequencies and amplitude of velocity disturbances u'/U_b under self-sustained limit cycle operation. (c) : Idealized representation of the burner geometry. Three lengths of the upstream manifold l_1 can be used together with three different length of the flame tube l_3.

the convergent unit is 60 mm. Combination of these elements yields twelve geometrical configurations. The equivalence ratio is set equal to $\phi = 0.7$ in all experiments but the flow velocity in the injection unit can be varied. Two values are investigated in this study corresponding to bulk injection velocities U_b = 2.67 m s^{-1} and U_b = 4.13 m s^{-1} determined in the injector pipe. The root mean square velocity disturbance u' is measured with a hot wire anemometer. This device is located in a cylindrical piece (15 mm in height) placed on the upstream side of the swirler. It has been demonstrated that the swirler has a very small effect on the time delay of the flow perturbations [29].

The response of the combustor to external acoustic perturbations is obtained when it is operating in a steady regime with a loudspeaker placed near the outlet section. This is used to generate harmonic perturbations and oscillations within the system are recorded with a microphone (M_0) located at the base of the burner. A second microphone (M_1) placed in front of the loudspeaker provides a reference signal. The response is then obtained by dividing the cross power spectral density examined at the driving frequency of the signals detected by microphones M_0 and M_1 by the power spectral density of the signal recorded by microphone M_1. This response is then used to determine the damping rate by examining the quality factor at the resonance peak.

The FDF is obtained by modulating the flame with a driver unit placed at the back end of the system and by simultaneously measuring the velocity oscillation with the hot wire anemometer placed on the upstream side of the swirler and the heat release rate perturbation by detecting the light intensity radiated by OH* radicals in the flame reaction zone. A previous study [29] indicates that the FDF determined using the axial velocity signal measured downstream the swirler at the flame base yields a similar result. It is known that for premixed flames at a constant equivalence ratio, the heat release rate is nearly

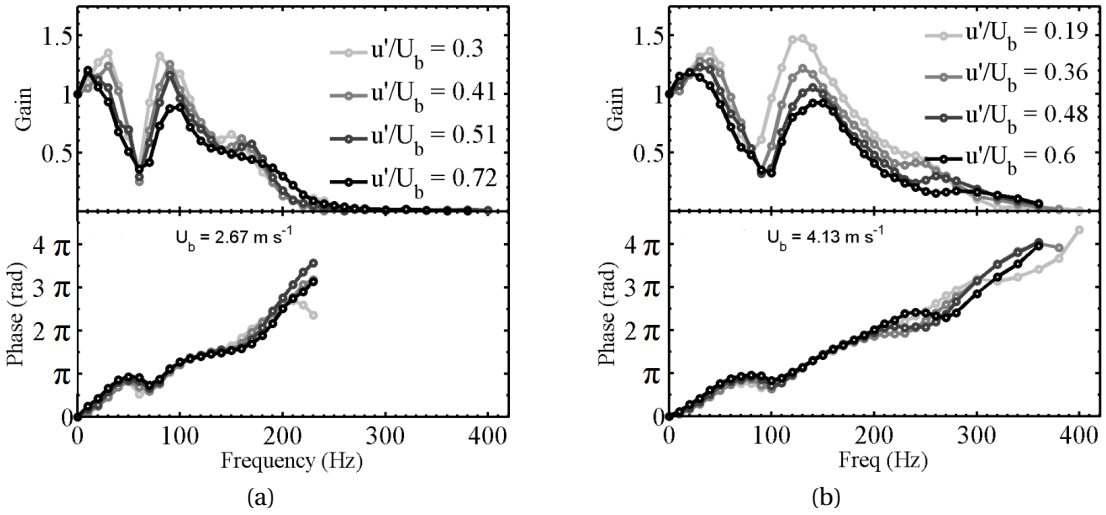

Figure 2: Flame Describing Functions for two operating points and for a range of perturbation velocities. Flame A on the left (U_b = 2.67 m s^{-1}) and flame B on the right (U_b = 4.13 m s^{-1}). Gains and phases are expressed as functions of frequency and ratio of amplitude of the root mean square velocity disturbance to the bulk velocity u'/U_b.

proportional to the light intensity I_{OH^*}. Light emission is collected by a photomultiplier located at 25 cm from the burner axis which integrates the global emission signal. This detector is equipped with a narrow bandpass filter centered on the main OH* peak light radiation in the near UV.

2 Experimental flame describing function

The flame response is here characterized by making use of the describing function [10]. This is accomplished by determining a set of transfer functions constituting the flame describing function (FDF). This quantity, defined by taking the ratio of the relative heat release rate fluctuation to the relative velocity fluctuation, is determined for a range of frequencies and for different levels of incoming velocity perturbations :

$$\mathscr{F}(\omega, u') = \frac{\dot{Q}'(\omega, u')/\overline{\dot{Q}}}{u'(\omega)/\overline{U}} \tag{1}$$

The heat release rate $\dot{Q}$ is deduced from OH* emission intensity and the axial velocity disturbance u' is measured with a hot wire anemometer. The flame describing function can be cast in the form of a complex number in terms of a gain G and a phase difference φ and expressed as :

$$\mathscr{F}(\omega, u') = G(\omega, u')\, e^{i\varphi(\omega, u')} \tag{2}$$

The gain corresponds to the level of response while the phase defines the time lag between velocity and emission signal. The FDFs presented in Fig. 2 pertain to flow with a bulk velocity U_b = 2.67 m s^{-1} and U_b = 4.16 m s^{-1} over a frequency range extending from 0 to 400 Hz and to four velocity modulation levels u'/U_b where u' corresponds to the root mean square (rms) perturbation level determined by the hot wire anemometer. Results are only presented for four discrete levels in Fig. 2 but intermediate perturbation amplitudes were also investigated.

For the first operating point (left of Fig. 2), the gain approaches one in the low frequency limit. It

decreases in a first range between 0 and 60 Hz to a value of less than 0.5. From 60 to 100 Hz, each curve features a peak. For all velocity disturbance levels, this peak is the maximum in the frequency range of interest. At 100 Hz, the flame response is the highest. Beyond 100 Hz and until 150 Hz, the gain drops again and reaches a value of 0.75 for most of the transfer function curves. From 150 Hz to 180 Hz, the gain increases but reaches a local maximum of about 0.7 for the smallest modulation level and 0.5 for the highest modulation level. Beyond 180 Hz the gain decreases in all cases and reaches a value which falls below 0.25. The phase in the bottom plot in Fig. 2 (b) increases nearly continuously with frequency from 0 to 250 Hz. Beyond 250 Hz, the phase is less smooth due to the low value of the gain in that frequency range and phase estimates become less reliable. The phase signal can be used to determine a global delay of the dynamical interaction between the incoming velocity modulation and the resulting heat release rate perturbation. If the phase varies in an approximately linear way with respect to frequency, it is possible to write $\varphi = \omega\tau_{cv}$ where $\omega = 2\pi f$. This can be used to determine a global time delay between a velocity perturbation measured at the hotwire location and the flame response which is found hereby independent of the frequency. For operating point A, a convective time delay : $\tau_{cv} = \varphi/2\pi f$ approximately equals to 5 ms in the frequency range of interest is calculated and corresponds to the time required by a disturbance to be convected to the flame and reach the flame edge. The dynamics observed for the second operating point B in the right part of Fig. 2 is quite similar to that found for point A shown in the left plot but with a shift in frequency. The minimum is around 90 Hz in the second case and the maximum around 130 Hz. It is possible to show that the describing functions for these two velocities are similar when they are plotted with respect to a Strouhal number based on the bulk flow velocity [27]. These FDF were also determined using a laser Doppler velocimeter at the flame base. A more complete analysis of the gain and phase evolution versus frequency is presented in [29].

3 Theoretical modeling

It is now interesting to show how the previous data can be included in a stability analysis. For this one has to link the flame describing function to the acoustics of the system. The simplified geometry of the burner is sketched in Fig. 1(c) which consist in three cylindrical parts. The first one has a length l_1 and corresponds to the upstream manifold part and to the first third of the convergent unit and its diameter is 65 mm. The second element has a length l_2 and is associated to the two others thirds of the convergent unit and to the injector. Its length is 116.7 mm and the diameter is 21.17 mm. This diameter corresponds to the hydraulic diameter of the injector pipe with the rod. Finally, the last part models the flame tube (70 mm in diameter and l_3 in length). Three cases are examined for l_1 : short, medium and long upstream manifold corresponding to respectively to 117.3 mm, 181.3 mm and 245.3 mm. The flame is established in a region where the flow area changes abruptly. On its upstream side this area is defined by the injection duct S_2, on its downstream side the area is that of the flame tube S_3. It is thus interesting to consider this geometry and derive the jump condition relating the upstream and downstream perturbated variables. This is accomplished by assuming that the flame is compact with respect to the wavelength.

It is convenient to start from a local equation obtained by combining mass and energy balance equations for a reactive medium. Since the flow velocities are small, the Mach number is low and the combustion region is nearly isobaric. One may also neglect the convective terms. Integrating the balance equation over the flame volume V, noting that the product $\rho_0 c_0^2$ (where ρ_0 is the density and c_0 the speed of sound) is constant across the flame and applying Green's theorem one obtains an expression for the integrated volumetric flux in terms of the global heat release fluctuations in the control volume. Using this expression between sections 2 and 3 in the system (plot Fig. 1(c)) and assuming that velocity perturbations are uniform in these sections one obtains the following jump condition :

$$S_3 u_3' - S_2 u_2' = \frac{\gamma - 1}{\rho_0 c_0^2} \dot{Q}' \tag{3}$$

This expression links velocity perturbations on the upstream and downstream sides of the flame to the unsteady heat release rate $\dot{Q}'$ integrated over the flame volume. The perturbated quantities appearing in this jump condition are not necessarily small. It is now possible to express the integrated heat release rate $\dot{Q}'$ in terms of the flame describing function defined previously (Eq.1) and write the jump condition as a function of the gain and phase of the FDF. By combining (Eq.1), (Eq.2) and (Eq.3), one finds :

$$S_3 u_3' - S_2 u_2' = \frac{\gamma - 1}{\rho_0 c_0^2} G e^{i\varphi} \overline{\dot{Q}} \frac{u_2'}{\overline{u}_2} \tag{4}$$

It is convenient to express the integrated mean heat release rate in terms of the fresh and burnt gas temperatures which in the present case correspond to T_2 and T_3 : $\overline{\dot{Q}} = \dot{m} c_p (T_3 - T_2)$ where $\dot{m} = \rho_2 \overline{u}_2 S_2$ is the total mass flow rate (we can observe that $\overline{u}_2$ corresponds to U_b). The product $\rho_0 c_0^2$ is a constant through the combustion region and can be evaluated in any of the sections belonging to the control volume V. It is convenient to use section 2 and express the sound velocity in that section : $\rho_0 c_0^2 = \rho_2 c_2^2 = \rho_2 \gamma r T_2$. Gathering these various results it is possible to obtain an expression for the ratio of the perturbated volume flow rates on the downstream and upstream sides of the flame $K(\omega, u_2') = (S_3 u_3')/(S_2 u_2')$:

$$K(\omega, u_2') = \left[1 + G e^{i\varphi} \left(\frac{T_3}{T_2} - 1 \right) \right] \tag{5}$$

Considering plane wave propagation in the different components of the system with amplitudes A_j and B_j, it is a simple matter to write that the pressure and volume flow rate perturbations are continuous at the successive area changes and use equation (Eq.5) to link the volumetric flow rate perturbations through the flame. These various equations combine with the boundary conditions at the system backplane (a rigid wall) and exhaust (an open end) yield a system of linear equations M × X = 0, where M is given by the following matrix :

$$\begin{bmatrix}
e^{ik_1 l_1} & e^{-ik_1 l_1} & -1 & -1 & 0 & 0 \\
1 & -1 & 0 & 0 & 0 & 0 \\
\frac{S_1}{\rho_1 c_1} e^{ik_1 l_1} & \frac{-S_1}{\rho_1 c_1} e^{-ik_1 l_1} & \frac{-S_2}{\rho_2 c_2} & \frac{S_2}{\rho_2 c_2} & 0 & 0 \\
0 & 0 & \frac{KS_2}{\rho_2 c_2} e^{ik_2 l_2} & \frac{KS_2}{\rho_2 c_2} e^{-ik_2 l_2} & \frac{-S_3}{\rho_3 c_3} & \frac{S_3}{\rho_3 c_3} \\
0 & 0 & 0 & 0 & e^{ik_3 l_3} & e^{-ik_3 l_3} \\
0 & 0 & e^{ik_2 l_2} & e^{-ik_2 l_2} & -1 & -1
\end{bmatrix}$$

where lengths l_1, l_2, l_3 are defined in Fig. 1 (c). k_j is the wavenumber in the j^{th} section and X is a vector of waves amplitudes in the various components of the system :

$\mathrm{X}^{\boldsymbol{T}} = [A_1 \quad B_1 \quad A_2 \quad B_2 \quad A_3 \quad B_3]$

This set of equations includes the flame describing function in the factor K defined previously (Eq. 5). Nontrivial solutions of this system correspond to a vanishing determinant. This defines the dispersion relation which now depends on the level of perturbations impinging on the flame. The determinant of this matrix can be derived analytically and takes the form :

$$\begin{aligned}
\mathrm{Det[M]} = & \frac{S_1}{\rho_1 c_1} \sin(k_1 l_1) \left[\frac{K(\omega, u_2') S_2}{\rho_2 c_2} \cos(k_2 l_2) \sin(k_3 l_3) + \frac{S_3}{\rho_3 c_3} \sin(k_2 l_2) \cos(k_3 l_3) \right] \\
& - \frac{S_2}{\rho_2 c_2} \cos(k_1 l_1) \left[\frac{S_3}{\rho_3 c_3} \cos(k_2 l_2) \cos(k_3 l_3) - \frac{K(\omega, u_2') S_2}{\rho_2 c_2} \sin(k_2 l_2) \sin(k_3 l_3) \right]
\end{aligned} \tag{6}$$

The complex roots $\omega = \omega_r + i\omega_i$ of the dispersion relation $\mathrm{Det[M}(\omega, u')] = 0$ are obtained numerically as a function of the perturbation level. This yields an angular frequency $\omega_r = \omega_r(u_2')$ and a growth rate $\omega_i = \omega_i(u_2')$ which both depend on the amplitude of velocity perturbations impinging on the flame. ω_r corresponds to $2\pi f$ where f is the oscillation frequency. Since flame transfer function were measured at four discrete levels, FTF at intermediate oscillation levels were interpolated linearly. One may thus trace the root locus as a function of the amplitude level in a diagram where the frequency is used as

ordinate while the growth rate is used as horizontal coordinate. In the absence of damping, the stability of the system is defined by the sign of $\omega_i(u_2')$. If this quantity is positive the oscillation grows and the system is unstable. However, the real system also features a certain amount of damping α. While this quantity is difficult to determine theoretically it can be estimated experimentally by measuring the resonance response of the system when it is submitted to an external forcing as explained in the experimental configuration section. The damping coefficient is then deduced (see the next section) from the frequency bandwidth of the acoustical response of the system to external modulations. Stability is then governed by the sign of $\omega_i(u_2') - \alpha$. In other words when the growth rate $\omega_i(u_2')$ exceeds the damping rate α, the oscillation amplitude increases. One also deduces that when $\omega_i(u_2') = \alpha$ the system reaches a limit cycle. This is used in what follows to analyze stability and determine the amplitude level at the limit cycle when the system features self-sustained oscillations.

4 Experimental results and comparison with predictions

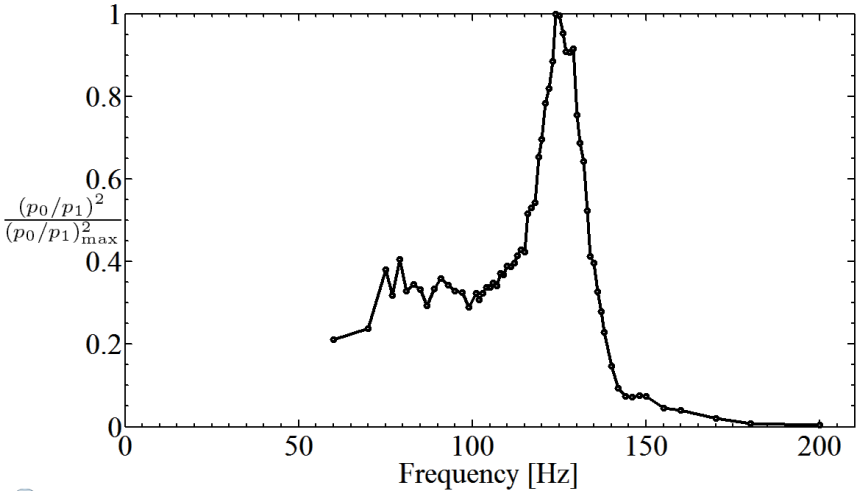

Figure 3: Experimental acoustic response of the combustor from $f = 0$ to $f = 200$ Hz. This curve is used to determine the damping coefficient α with $\alpha = \pi\Delta f$.

4.1 Experimental measurements of the system damping

As indicated in the previous section, the growth rate must be compared to the damping coefficient to determine the stability of the system. This coefficient can be estimated from a resonance response by submitting the system to an external excitation and measuring the resonance sharpness. It is important to operate under stable conditions to obtain the frequency response. This can be achieved by making use of the long upstream manifold equipped with a 100 mm flame tube. This response is plotted in Fig. 3 ans is obtained with the short upstream manifold and the 100 mm flame tube. From the frequency response one finds the half power points which give the frequency bandwidth Δf. Assuming that the system is analogous to an harmonic oscillator, one deduces the damping coefficient $\alpha \simeq \pi\Delta f$. It is assumed that the damping coefficient remains close to this value for the other burner geometries and is not frequency dependent. This is reasonable if the main contribution to damping is related to the area changes between the upstream manifold and injector and between the injector and the flame tube. The typical value of the damping rate is $\alpha \simeq 55$ s^{-1}. This damping is much larger than that found for the same configuration but in the absence of flow and reaction. The measurement itself is imperfect and one should take into account a possible error bar $\pm$ 10 s^{-1}.

4.2 Self-sustained oscillations

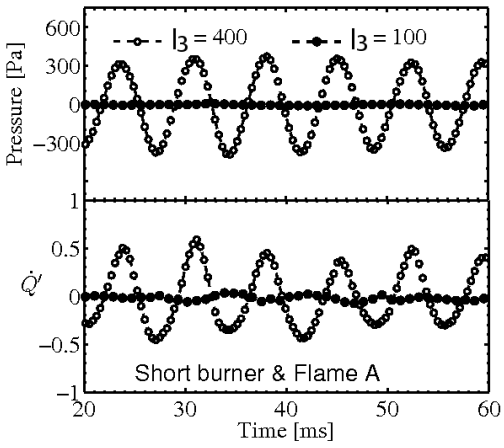

Figure 4: Time pressure evolution in Pascals measured at the base of the combustor with the microphone M_0 and heat relase rate fluctuation $\dot{Q}'$ measured with a photomultiplier. The geometrical configuration is based on the short upstream manifold for flame A and two lengths of the flame tube are matched : $l_3 = 100$ mm and $l_3 = 400$ mm. The short flame tube is stable while the long one is unstable.

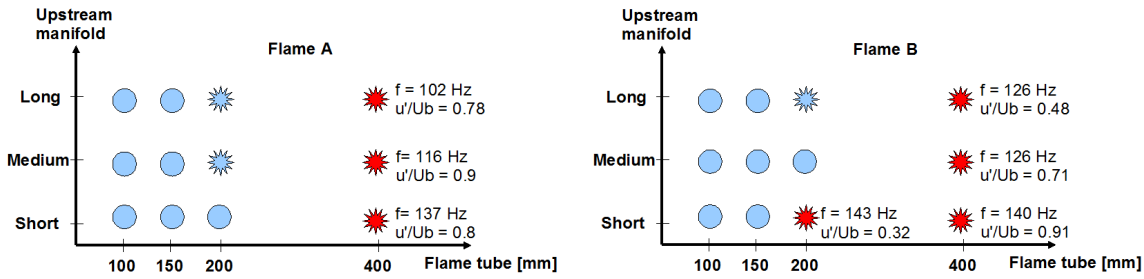

Figure 5: Combustor stability map for both flames (a) for flame A and (b) for flame B. The stable configurations are in blue circles while reds stars indicate a high level of rms pressure which corresponds to a self-sustained oscillation of the system. Blues stars corresponds to slightly unstable cases. When the system is unstable, the frequency at the limit cycle and the relative oscillation amplitude are given.

Self-sustained oscillations are characterized by the root mean square of the pressure fluctuation at the base of the upstream manifold. The signal is obtained with the microphone M_0, see Fig. 1 (b). When the rms pressure level is low and broadband, the system is operating in a stable mode. It is oscillating when most of the power is concentrated in a narrow band of frequencies and when the rms pressure exceeds a threshold value which corresponds to the typical noise level in the system and in the present case can be taken equal to 10 Pa. This is illustrated in Fig. 4 which displays temporal evolutions of heat release rate fluctuation and pressure inside the upstream manifold for one stable and one unstable case. The geometry is based on the short upstream manifold for the operating point A and the length of the flame tube is varied from $l_3 = 100$ mm to $l_3 = 400$ mm. These signals indicates that the long flame tube leads to an unstable oscillation while the flame is stable when the flame tube is short for the operating point A.

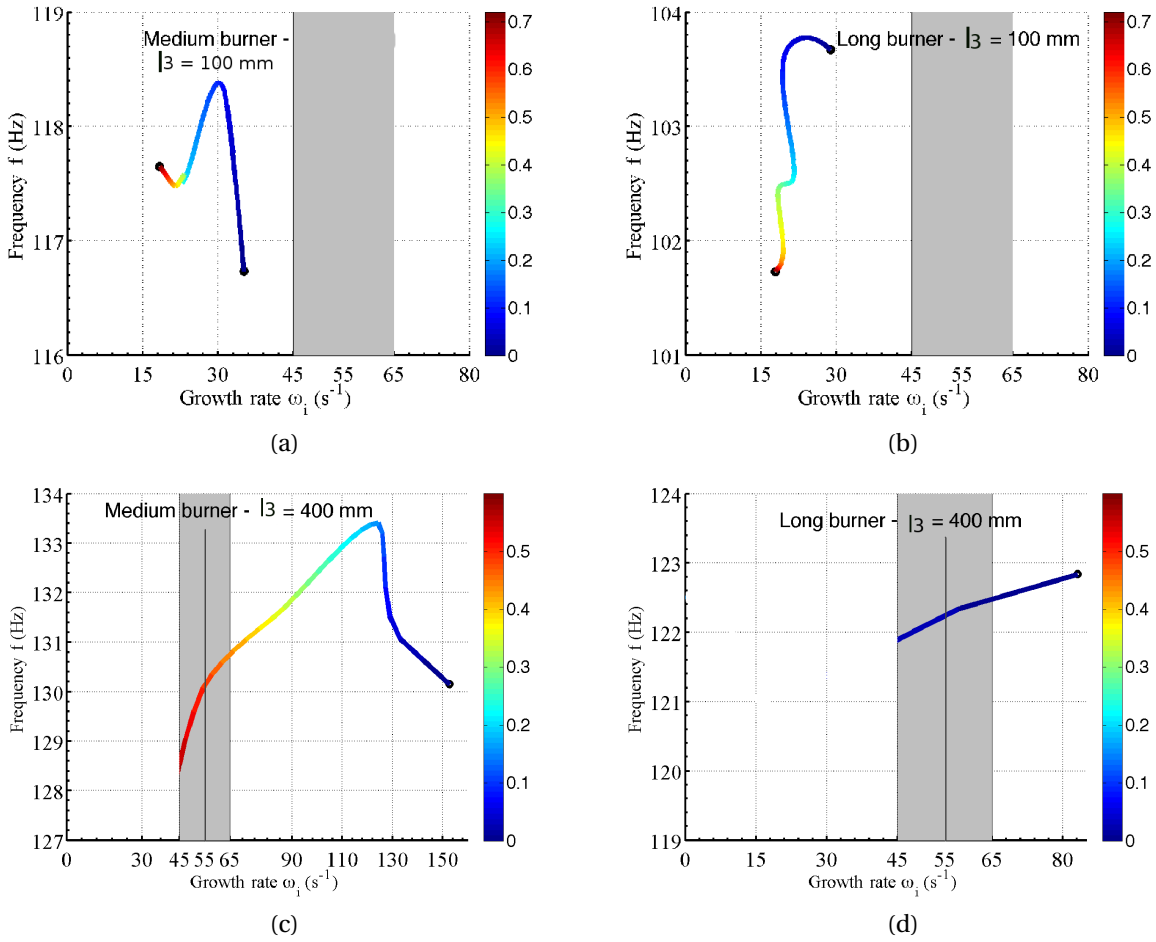

Figure 6: Frequency - Growth rate trajectories plotted as a function of the velocity disturbance level u'/U_b. The value of the damping coefficient α is shown in the form of a grey region representing the error bar on this quantity. The root locus is plotted on a color scale as a function of the relative fluctuation u'/U_b. (a) and (b) respectively correspond to a system equipped with the medium and long upstream manifold and for a confinement tube length $l_3 = 100$ mm. Flow conditions are those of flame A. The trajectory is on the left of the damping region indicating that the system is stable. (c) and (d) respectively correspond to a system equipped with the medium and long upstream manifold and for a confinement tube length $l_3 = 400$ mm. Conditions are those of flame B. The trajectory is on the right of the damping region indicating that the system is unstable. The limit cycle is reached for $u'/U_b \simeq 0.5$ on the left and $u'/U_b \simeq 0.15$ on the right.

Results of systematic experiments are plotted in Fig. 5 for flames A and B. The stars are displayed as a function of geometrical parameters of the configuration : flame tube length and upstream manifold size. Results are given for operating points A and B corresponding to two different bulk velocities in the injection unit. Blue circles indicate stable configurations while red stars indicate self-sustained instabilities. Blues stars corresponds to slightly unstable cases. Both figures indicate when the system is stable or unstable for flames A and B. When the system is equipped with a 400 mm flame tube, it is unstable for all sizes used for the upstream manifold and for both operating points A and B. One can observed that for some cases, the amplitudes of velocity u'/U_b is very high. As the bulk velocity U_b is used, it can slightly overestimated the real level of fluctuation.

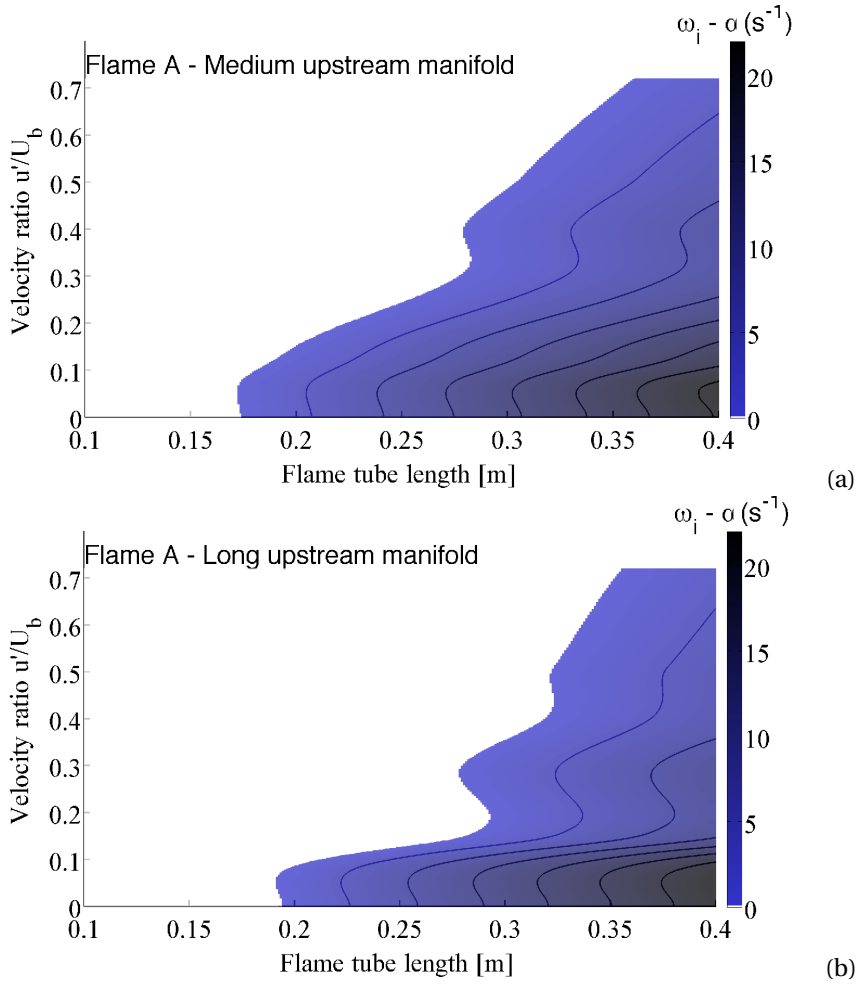

Figure 7: Stability maps of the burner for flame A. (a) corresponds to the medium upstream manifold while (b) corresponds to the long upstream manifold.

4.3 Limit cycles

Results of calculations are plotted in Fig. 6. Each plot shows the root locus $\omega_i(u_2'), f(u_2')$ when the relative velocity fluctuation level upstream of the flame is progressively increased. The error bar on the damping is also shown in the form of a vertical gray region centered around 55 s^{-1}, the damping measured from results plotted in Fig. 3 . When the trajectory is on the left of the estimated damping, the system is stable. It corresponds to negative values of $\omega_i(u_2') - \alpha$ meaning that the pressure fluctuation is damped as a function of time. When it begins on the right of the region corresponding to the estimated damping the system is unstable and reaches a limit cycle at the cross point between the trajectory and the vertical region corresponding to α with the error bar in gray.

The root locus is plotted as a function of frequency f expressed in Hertz and growth rate ω_i given in s^{-1} as a function of the velocity disturbance amplitude. Four cases are described, two for flame A and the others for flame B. The first cases (a) and (b) start with a growth rate which is below $\alpha = 55$ s^{-1} and at frequencies near 111 Hz and 104 Hz. The trajectory always remains on the left of the damping value indicating that the system is stable. This is indeed what is observed experimentally as shown in Fig. 5.

For flame B with the medium upstream manifold and $l_3 = 400$ mm, Fig. 6 (c) indicates that the tra-

Upstream manifold (burner)	Medium	Long
Experimental frequency	126 Hz	125 Hz
Predicted frequency	130 Hz	122 Hz
Experimental velocity amplitude	0.71	0.4
Predicted velocity amplitude	0.55	0.15

Table 1: Comparison between predictions and experiments at limit cycle for operating point B and flame tube length l_3 = 400 mm.

jectory begins on the right of α and that it crosses the damping boundary for a relatively high value of u'/U_b. The limit cycle is reached for a frequency of 130 Hz for $u'/U_b \simeq 0.55$. This is consistent with experimental observations indicating that the system oscillates at f = 126 Hz and that the amplitude at the limit cycle is $u'/U_b = 0.71$. For flame B with the long upstream manifold and l_3 = 400 mm, in Fig. 6 (d), the growth rate also exceeds the damping coefficient α at the beginning but the trajectory crosses the damping boundary at a much lower value of the relative velocity disturbance $u'/U_b \simeq 0.15$. This is underestimated with what is shown in Fig. 5 where the level of oscillation reaches $u'/U_b = 0.4$. One explanation of this underestimation is that the rms value is determined in the prediction with pure harmonic signals while background noise is superimposed in the experiments due to turbulent flow. This may lead in the experiments to slight differences with higher rms values for limit cycles at moderate amplitudes. The predicted frequencies at the limit cycle (130 Hz for case (c) and 122 Hz for case (d)) are also in good agreement with experimental measurements which respectively indicate 126 Hz and 125 Hz. All results are gathered in Table 1.

It is interesting to determine the evolution of the growth rate minus the damping coefficient $\omega_i - \alpha$ as a function of the velocity amplitude and the length of the flame tube. When the value of $\omega_i - \alpha$ is equal to zero, the system reach the limit cycle. In Fig. 7, the stability maps for flame A are plotted for two lengths of the upstream manifold. These plots can be used to predict the stable or unstable behavior of a configuration. With the medium upstream manifold (Fig. 7(b)), it is observed that for a flame tube of 0.17 m in length the combustor is stable. Increasing the flame tube length, the amplitude of the velocity disturbance at limit cycle increases to reach very high levels. It appears that these high amplitude levels are a limit of the limit cycle and corresponds to the values theoretically assumed in a previous work [7] to explained the saturation in combustion instability.

Conclusion

This article focuses on the analysis of combustion instabilities of swirling flames in a configuration idealizing typical situations encountered in practice. The geometry can be varied by changing the lengths of the upstream manifold and flame tube. The flame describing function determined experimentally is used to represent the nonlinear response of the combustion process to velocity perturbations of various levels. These data are used in combination with an acoustic transfer matrix analysis to derive a nonlinear dispersion relation. This is then exploited to determine the frequency and growth rate of perturbations in the system as a function of the amplitude of velocity perturbations on the upstream side of the flame. Values of the growth rate are then compared to the damping coefficient of the system obtained from separate experiments to determine stability or instability and obtain the amplitude when the system oscillates at a limit cycle. Theoretical predictions retrieve experimental observations validating the FDF methodology applied to the case of confined swirling flames.

Acknowledgment

This study is part of the MICCA project supported by the Agence Nationale de la Recherche. Contract number : ANR-08-BLAN-0027-01.

References

[1] Crocco, L., *Research on combustion instability in liquid propellant rockets*, Proceedings of the Combustion Institute, Vol. 12, 1968, pp 85-99

[2] Putnam, A.A., *Combustion driven oscillations in industry* , Elsevier, New-York

[3] Culick, F.E.C., *Dynamics of combustion systems : fundamentals, acoustics and control*, Proceedings of the RTO/VKI special course on “Active control of engine dynamics", 2001, pp 6.1-6.133

[4] Candel, S., *Combustion Dynamics and Control : Progress and Challenges*, Proceedings of the Combustion Institute, 2002, pp 1-28

[5] Lieuwen, T. and Zinn, B.T., *The role of equivalence ratio oscillations in driving combustion instabilities in low NO_x gas turbines*, Proceedings of the Combustion Institute, 1998, pp 1809-1816

[6] Wicker, J.M., Greene, W.D., Kim, S.I. and Yang, V., *Triggering of longitudinal combustion instabilities in rocket motors: nonlinear combustion response*, Journal of Propulsion and Power, 1996, Vol. 12, pp 1148-1158

[7] Dowling, A.P., *Nonlinear self-excited oscillations of ducted flame*, Journal of Fluid Mechanics, 1997, Vol. 346, pp 271-290

[8] Dowling, A.P., *A kinematic model of ducted flame*, Journal of Fluid Mechanics, 1997, Vol. 394, pp 271-290

[9] Lieuwen, T. and Neumeier, Y., *Nonlinear pressure-heat release transfer function measurements in a premixed combustor* , Proceedings of the Combustion Institute, 2002, Vol. 29, pp 99-105

[10] Noiray, N., Durox, D., Schuller, T. and Candel, S. , *A unified framework for nonlinear combustion instability analysis based on the describing function* , Journal of Fluid Mechanics, Vol. 615, 2008, pp 139-167

[11] Noiray, N., Durox, D., Schuller, T. and Candel, S. , *A method for estimating the noise level of unstable combustion based on the flame describing function*, International Journal of Acoustics, 2009, Vol. 8, pp 157-176.

[12] Lieuwen, T. and Neumeier, Y., *Thermoacoustics stability chart for high-intensity gas turbine combustion systems* , Combustion Sciences and Technology, 2002, Vol. 174, pp 99-128

[13] Broda, J.C., Seo, S., Santoro, R.J., Shirhattikar, G. and Yang, V., *An experimental study of combustion dynamics of a premixed swirl injector* , Proceedings of the Combustion Institute, 2002, Vol. 27, pp 1849-1856

[14] Lilley, D.G., *Swirl flows in combustion : a review*, AIAA Journal, 1977, 15, pp 1065-1078

[15] Syred, N., *A review of oscillation mechanisms and the role of the precessing vortex core (PVC) in swirl combustion systems*, Progress in Energy and Combustion Science, 2006, 32, pp 93-161

[16] Thumuluru, S.K., Ma, H.H. and Lieuwen, T., *Measurements of the flame response to harmonic excitation in a swirl combustor*, AIAA Aerospace Sciences Meeting and Exhibit, Reno, Nevada, AIAA Paper 2007-0845, 2007

[17] Durox, D., Schuller, T. and Candel, S., *Combustion dynamics of inverted conical flames*, Proceedings of the Combustion Institute, Vol. 30, 2005, pp 1717-1724

[18] Balachandran, R., Ayoola, B. O., Kaminski, C. F., Dowling, A. P. and Mastorakos, E., *Experimental investigation of the nonlinear response of turbulent premixed flames to imposed inlet velocity oscillations*, Combustion and Flame, Vol. 143, 2005, pp 37-55

[19] Lawn, C.J., *Thermo-acoustic frequency selection by swirled premixed flames*, Proceedings of the Combustion Institute, Vol. 28, 2000, pp 823-830

[20] Külsheimer, C. and Büchner, H., *Combustion dynamics of turbulent swirling flames*, Combustion and Flame, Vol. 131, 2002, pp 70-84

[21] Kang, D.M., Culick, F.E.C. and Ratner, A., *Combustion dynamics of a low-swirl combustor*, Combustion and Flame, Vol. 151, 2007, pp 412-425

[22] Fritsche, D., Füri, M. and Boulouchos, K., *An experimental investigation of thermoacoustic instabilities in a premixed swirl-stabilized flame*, Combustion and Flame, Vol. 151, 2007, pp 29-36

[23] Gentemann, A., Hirsch, C., Kunze, K., Kiesewetter, F., Sattelmayer, T. and Polifke, W., *Validation of flame transfer function reconstruction for perfectly premixed swirl flames*, Proceedings of ASME Turbo Expo 2004, GT2004-53776, Vienna, Austria, 2004.

[24] Hirsch, C., Fanaca, D., Alemela, R., Polifke, W. and Sattelmayer, T., *Influence of the swirler design on the flame transfer function of premixed flames*, Proceedings of ASME Turbo Expo 2005, GT2005-68195, Reno, USA, 2005

[25] Armitage, C.A., Balachandran, R., Mastorakos, E. and Cant, R.S., *Investigation of the nonlinear response of turbulent premixed flames to imposed inlet velocity oscillations*, Combustion and Flame, Vol. 146, 2006, pp 419-436

[26] Bellows, B.D., Bobba, M.K., Seitzman, J.M. and Lieuwen, T., *Nonlinear flame transfer function characteristics in a swirl-stabilized combustor*, Proceedings of the ASME Turbo Expo 2003, GT2006-91119, Vol. 129, 2003, pp 954-961

[27] Palies, P., Durox, D., Schuller, T., Morenton, P., Candel, S., *Dynamics of premixed confined swirling flames* , Comptes Rendus Mecanique, Vol. 337, 2009, pp 395–405

[28] Palies, P., Durox, D., Schuller, T., Candel, S., *Combustion dynamics of a swirling premixed confined flame*, Proceedings of the 4th European Combustion Meeting, Vienna, Austria, 2009.

[29] Palies, P., Durox, D., Schuller and Candel, S., *The combined dynamics of swirler and turbulent premixed swirling flames*, Combustion and Flame (In Press), doi : 10.1016/j.combustflame.2010.02.011

[30] Nicoud, F., Benoit, L., Sensiau, C. and Poinsot, T., *Acoustic mode in combustors with complex impedances and multidimensional active flames*, AIAA Journal, Vol. 45, 2007, pp 426-441

[31] Stow, S. and Dowling, A., *Thermoacoustic oscillations in an annular combustor* , ASME paper GT0037, ASME Turbo Expo 2001, 2001

[32] Schuermans, B., Guethe, F., Pennel, D., Guyot, D. and Paschereit, C.O. *Thermoacoustic modeling of a gas turbine using transfer functions measured at full engine pressure*, Proceedings of the ASME Turbo Expo 2009, GT2009-59605, 2009

[33] Kang, D.M., Culick, F.E.C. and Ratner, A., *Combustion instabilities in liquid-fueled propulsion systems : an overview*, AGARD Meeting 72B PEP, 1987

[34] Selle, L., Lartigue, G., Poinsot, T., Koch, R., Schildmacher, K.U., Krebs, W., Prade, B., Kaufmann, P. and Veynante, D., *Compressible large eddy simulation of turbulent combustion in complex geometry on unstructured meshes*, Combustion and Flame, Vol. 137, 2004, pp 489-505